Monitoring casing corrosion of legacy wells using CSEM: Implications for large-scale energy and CO_2 storage projects in shut-down hydrocarbon fields

Simone Zonetti[1], Bastien Dupuy[2], Benjamin Emmel[2], and Anouar Romdhane[3]

https://doi.org/10.1190/tle42120808.1

Abstract

Large-scale CO_2 and energy storage is a mandatory part of the green shift to reduce CO_2 emissions and limit consequences of climate change. Large-scale storage will require the use of shut-down depleted hydrocarbon fields to take advantage of well-characterized reservoirs and cap rocks. Thanks to extensive data from historical hydrocarbon production, the uncertainties related to storage capacity, injectivity, and containment are limited. However, legacy exploration and production infrastructure, and especially legacy wells, are the main threat for possible fluid leakage toward the surface. Such legacy wells are numerous and penetrate the full rock column. In this paper, we describe a workflow to screen and monitor legacy wells in the shut-down Frigg Field in the North Sea. By using numerical modeling of electromagnetic (EM) field propagation in one of the Frigg Field wells, we explore the complex interactions of fields, currents, and well structure in the presence of corrosion. The corrosion is implemented as a change in the electrical conductivity of the innermost steel casing at different depths along the structure. To enhance probing depth, we plug the dipole source (1 km long) into the casing at the seafloor and excite the casing as an antenna. We find that at moderate levels of corrosion, the current distribution is significantly modified with respect to the uncorroded case. This generates a signal that propagates and can be observed at the seafloor in the numerical results. Other elements of the well geometry (e.g., concentric overlapping cement casings) have their own effect on the signal. This leads the possibility of estimating the location of the corroded area within the well geometry. These results suggest that by relaxing some of the model's approximations and implementing realistic transmitters, it will be possible to evaluate and optimize controlled-source EM survey strategies for detecting and monitoring corrosion levels.

Introduction

In the European Green Deal, the North Sea plays a central role in reaching climate neutrality by 2050. The North Sea is envisioned as a hub (Thommessen et al., 2021) to (1) provide renewable energy from offshore wind farms; (2) produce green hydrogen generated by renewable energy; and (3) store CO_2 and energy (e.g., H_2, compressed air, or heat) in deep rock formations due to its large storage capacity and existing infrastructure (Lothe et al., 2019; NMPE, 2020; Osmond et al., 2022). The Norwegian Continental Shelf (NCS) has an estimated CO_2 storage capacity of more than 80 Gt in different geologic formations (Norwegian Petroleum Directorate, 2014a). Geologic reservoirs that can serve as storage in the NCS include saline aquifers and depleted shut-down oil and gas fields. Historical oil and gas regions are the most obvious candidates for fast development of subsurface storage because they have well-characterized proven reservoir quality and sealing cap rocks. There are three additional advantages. (1) They are usually underpressured, enabling better storage capacity by avoiding limitations due to pressure buildup (e.g., Ringrose and Meckel, 2019) and enabling less risk of geomechanical failure due to CO_2 injection. (2) There is likely more control on plume migration, and conformance monitoring is easier (Eliasson et al., 2021). (3) There are possibilities to use infrastructure in place (e.g., pipelines, wells, platforms, etc.), thus reducing initial investment costs. Consequently, the shut-down fields are locations that can be utilized for storage purposes relatively quickly (e.g., Porthos and Aramis projects in the Netherlands [e.g., Akerboom et al., 2021]).

On the other hand, challenges arise with the use of shut-down fields for CO_2 or energy storage. These include the effect of residual oil and/or gas that will still be present and may lead to chemical interactions with the injected fluids (Sun et al., 2020; Hamza et al., 2021). Residual hydrocarbons (especially gas) are also problematic for the interpretation of time-lapse seismic (which is the backbone for monitoring) due to the weak contrast between gas-brine- and CO_2-brine-saturated sands (Urosevic et al., 2010; Hannis et al., 2017). However, the main challenge relates to old legacy wellbores that may slow the shift from an oil and gas producing field to a storage field. Thousands of wells (8000 wells in the NCS and 6500 wells in the Norwegian North Sea) have been drilled in the region (Figure 1). Some of the wells are permanently or temporarily abandoned, including exploration wells from the 1970s to the 1990s. This happened long before modern safety and environmental regulations for well plugging and abandonment were implemented (e.g., NORSOK D-10, 2004). When a well is plugged and abandoned (P&A), cement plugs are built at a minimum of three locations (Vrålstad et al., 2019): (1) directly above the main reservoir, (2) in each potential flow zone, and (3) close to the surface (environmental plug). In addition to P&A regulations, regulations for CO_2 storage require an assessment of leakage risks, monitoring, and mitigation possibilities for legacy wells (e.g., ISO, 2022). Legacy wells have been identified as the main leakage path for fluids drilled or injected into the subsurface

[1]SINTEF Digital, Oslo, Norway. E-mail: simone.zonetti@sintef.no.
[2]SINTEF Industry, Trondheim, Norway. E-mail: bastien.dupuy@sintef.no; benjaminudo.emmel@sintef.no.
[3]Formerly, SINTEF Industry; presently, Equinor ASA, Stjørdal, Norway. E-mail: mromd@equinor.com.

(Gasda et al., 2004). The Intergovernmental Panel on Climate Change Special Report on Carbon Capture and Storage (IPCC, 2005) indicates that potential migration and release pathways from geologic reservoirs include inadequately completed and/or abandoned wells. The associated mechanisms for migration and release pathways may include degradation of the cap rock or the wells from reactions with acidic formation waters (typically brine that is partially saturated with CO_2).

The leakage risks are related to a potential lack of control during P&A completion or to degradation of the well elements over time after P&A. For example, cement plugs are prone to degradation due to pH changes of the reservoir brine (Bertolini et al., 2003) or due to stress and pressure changes in the reservoir and cap rock. If the casing is left in place when the well is abandoned, the casing steel can be subject to corrosion due to corrosive fluids such as brine mixtures with CO_2 (e.g., Choi et al., 2013). Preferred paths for fluid leakage in wellbores are at the interfaces between well elements, especially (1) between the rock formation and outer casing cement, (2) between the outer casing cement and casing, (3) between the casing and cement plug, and (4) through the cement plugs themselves (Figure 1c).

Legacy wells also constitute an asset, not only a threat (IPCC, 2005), for large-scale CO_2 and H_2 storage. Drilling of the underground is necessary to finely characterize and validate a storage area. Log and core data, recorded while drilling exploration wells, provide knowledge of potential reservoirs and their sealing abilities including the full rock formation columns (not only the oil and gas targets). Legacy wells and related data are consequently crucial for characterization of the reservoir and overburden of future storage complexes. To derisk the storage complex and gain a permit for large-scale storage in the NCS (Norwegian Petroleum Directorate, 2014b), it is mandatory to assess the status of legacy wells and monitor them over time to ensure that their elements are not being damaged and no leakage is occurring. Legacy wells with an uncertain integrity status are a financial risk for potential operators. If legacy wells must be re-entered to secure the storage unit, the costs may be comparable to the cost of drilling a new well. In addition to regulations and operational costs, legacy wells pose a challenge regarding public acceptance of underground fluid storage projects, requiring reliable monitoring of potential leakages.

A legacy well screening and monitoring workflow for CO_2 storage in aquifers has been demonstrated for the Smeaheia site (Romdhane et al., 2022a). In this paper, we focus on Frigg Field (Figure 1), a shut-down and decommissioned gas field located in the central part of the North Sea (Total, 2011). The first step aims at identifying the legacy wells in the area and screening the old well completion and P&A reports. This stage allows us to classify the legacy wells, depending on information available about their status at the time of drilling and abandonment. Several criteria are assessed including P&A status, report quality, verification job, amount of cement injected, and number and location of cement plugs (Emmel and Dupuy, 2021). Alternative approaches are proposed in the literature (Pawar et al., 2021; Cahill and Samano, 2022; Koning et al., 2023). When the wells are assessed and classified, we select the critical ones that need further investigation (e.g., active monitoring and surveillance). Because the wells are abandoned, the wellhead is usually cut and buried under the seafloor. With the borehole being inaccessible and very expensive to re-enter, we focus on noninvasive monitoring techniques. Geophysical approaches, such as seismic and controlled-source electromagnetic (CSEM), are commonly used in oil and gas exploration and reservoir monitoring and can provide information about the well status without the need to re-enter. Preliminary

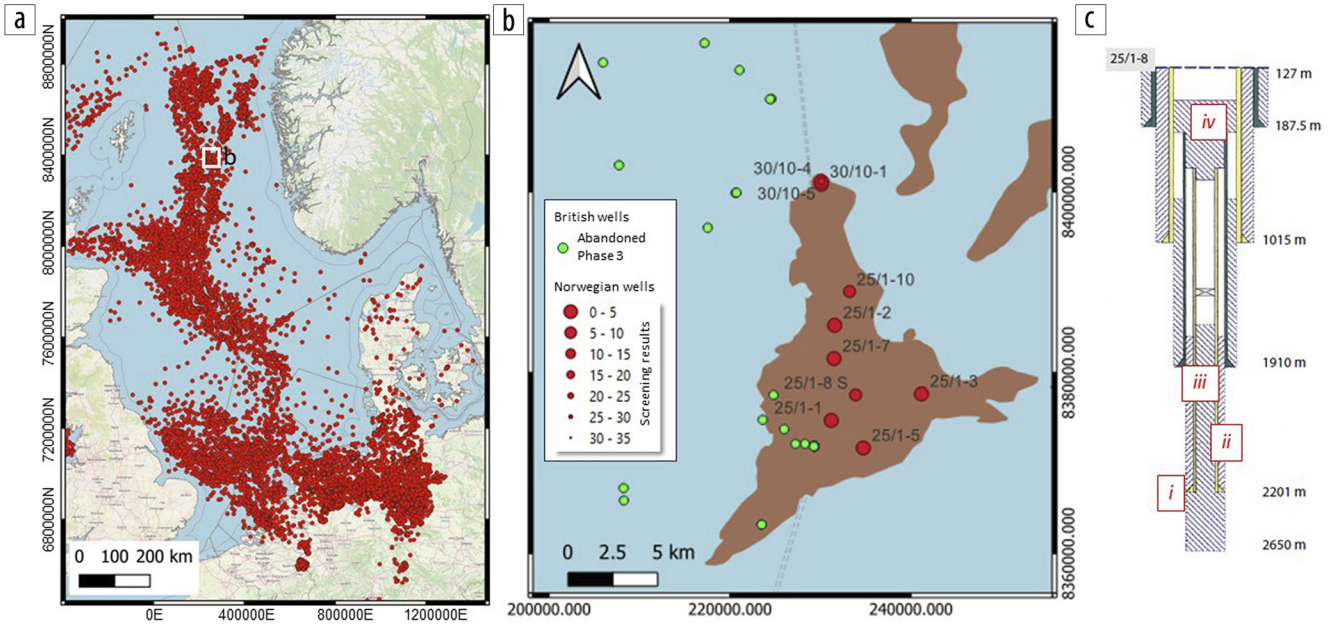

Figure 1. (a) Location of the study area in the North Sea (white box). Red dots are oil and gas well locations. (b) Map of Frigg Field with well locations. For the British part (green dots), the abandonment status is given. For the wells located in the Norwegian economic zone (red dots), the well identifiers are given. The size of the red dots relates to screening results for P&A status following the approach given in Emmel and Dupuy (2021). (c) Plugging and abandonment plan for well 25/1-8 located in the center of Frigg Field (Norwegian Petroleum Directorate, 1991). Numbers indicate preferential leakage paths along a well structure.

work by Romdhane et al. (2022b) shows that corrosion of shallow sections of casing can be detected with CSEM. Wilt et al. (2020) demonstrate that using the casing as an antenna for time-domain reflectometry surveys is relevant to enhance the probing depth for casing corrosion in onshore wells.

We will first describe the shutdown Frigg Field, with some details of storage capacity and examples of reservoir fluid migration in the case of injection of CO_2. Then, the existing legacy exploration wells are assessed and classified, one of which is located in the center of the field and selected for detailed analysis. Finally, we build a numerical model of the selected legacy well to test the ability of EM signals to detect corroded casings.

Frigg Field storage capacities

Frigg Field is located in the central part of the North Sea (Figure 1a). Production started in 1977 after the first discovery in 1971. The field was shut down in 2004 after 27 years of production from a reservoir in the Frigg Formation at a depth of about 1900 m. Final decommissioning of the facilities was completed in 2010 (Total, 2011).

Based on hydrocarbon production data, the storage capacities for CO_2 (Holloway et al., 1996) and H_2 (Emmel et al., 2023a) can be calculated. During its lifetime, the Norwegian part of the field produced 115.8 billion standard cubic meters (Sm^3) of gas and 0.114 million Sm^3 of condensate (Norwegian Petroleum Directorate, 2023). Using the parameters given in Table 1, theoretical storage capacities of 355 to 422 Mt for CO_2 and 5.9 to 7.6 Mt for H_2 are estimated. The mass of H_2 can be transferred to an energy equivalent of 197 to 299 TWh. Norway's CO_2 emissions in 2022 was 48.9 Mt (Statistics Norway, 2023a) and energy consumption was 218 TWh (Statistics Norway, 2023b). Consequently, Norway's CO_2 emissions for approximately eight years can be stored in Frigg Field. In case of energy storage in the form of H_2 injection, approximately one year of Norway's energy can be stored in Frigg Field.

By using a simplified reservoir model based on publicly available wellbore data and map information, parameterized with data given by De Leebeeck (1987), we run reservoir modeling simulations with variations in the injection well location (Figure 2). We show that, independent from the injection well location, CO_2 will reach most of the legacy wells (Romdhane et al., 2022b). Frigg Field capacity estimates for storage of CO_2 or H_2 are substantial. However, before using Frigg Field as a storage site, a detailed analysis of legacy wells is required.

Table 1. Theoretical CO_2 and H_2 storage capacities for Frigg Field and parameters used for the calculations. The mass of H_2 is converted to potential energy by using heating values of 33.33 and 39.4 kWh/kg (Emmel et al., 2023b).

Original in-place free gas	(billion Sm^3)	150.2	Oil density	(kg/m^3)	0.834
Produced gas	(billion Sm^3)	116.62	H_2 density at res. cond.	(kg/m^3)	10.072–12.906
Produced condensate	(million Sm^3)	0.46	CO_2 density at res. cond.	(kg/m^3)	604–718
Remaining gas	%	22.36	CO_2 storage capacity	Mt	355–422
Res. pressure	bar	150–197	H_2 capacity	Mt	5.93–7.59
Res. temperature	(°C)	60	Energy equivalent H_2	TWh	197.65–299.04
GEF		198			

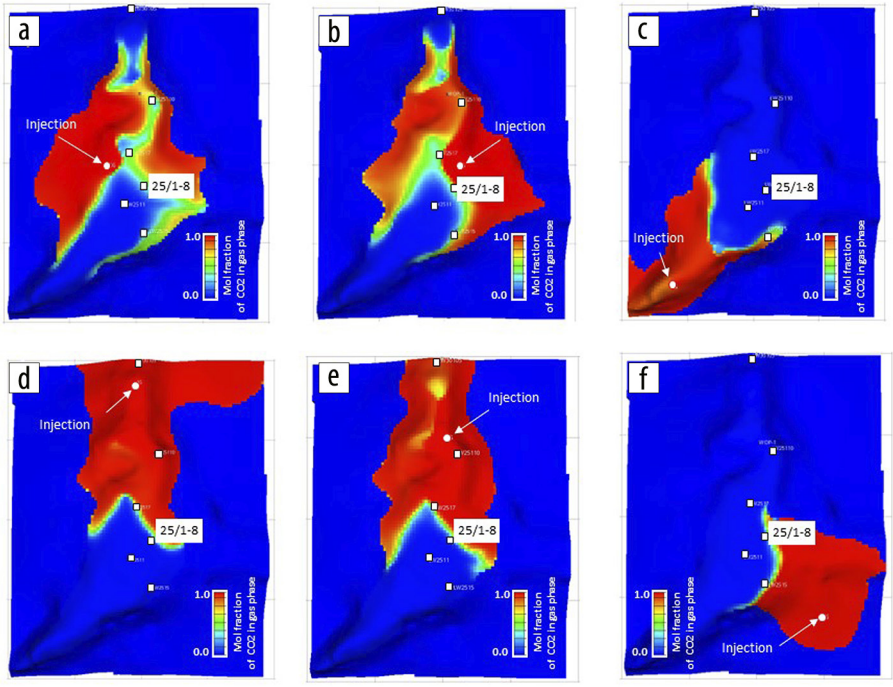

Figure 2. (a)–(f) Results of reservoir modeling. Mole fraction of CO_2 in the gas phase at the top of the Frigg Formation using different injection locations after 50 years of injection of 250 Mt of CO_2. The approximate positions of legacy wells in the center of the field are shown with white boxes, and varying locations of the injection wells are marked with white dots. The model's width is approximately 17.5 km.

Well screening

In Frigg Field, 67 wells were drilled according to the available database, including 10 exploration wells with publicly available documentation on the completion process. We only screened legacy exploration wells because (1) the data are publicly available, (2) they are usually the oldest wells drilled in an unknown field, (3) they penetrate the full rock column even below the reservoir unit, and (4) P&A has been executed without detailed knowledge of the hydrocarbon reservoir target and without taking into account any possible future fluid storage operations. Emmel et al. (2023b) use the available data to screen the P&A status of exploration wells in Frigg Field following the method described in Emmel and Dupuy (2021). This method analyzes the data reported from the operator to the Norwegian Petroleum Directorate. These

Table 2. Summary of screening results of the 10 exploration wells of Frigg Field. Results are given for single criteria and total score. Status is for the last re-entry stage. Abbreviations are as follows (Emmel and Dupuy, 2021): wb_name = wellbore name; sc_status = status description for exploration wells from NPD; sc_entryYear = year of drilling (related to regulations); sc_plug_da = reporting of plugging operations to the authorities; sc_plug_ab = score for finishing date reported to the authorities; sc_report = report quality; sc_cem_job = casing cement job evaluation; sc_cs_ver = casing cement job verification; sc_plug_jo = whether abandonment, reservoir, and surface plugs are in place; sc_plug_len = plug length; sc_pl_ver = whether there was tagging or weight testing of plugs; sc_mil = milling of casing to improve cement integrity; and sc_ind_leak = whether there was leakage indicated by secondary measurements.

wb_name	sc_ status	sc_ entryYear	sc_plug_ da	sc_plug_ ab	sc_ report	sc_cem_ job	sc_cs_ ver	sc_plug_ jo	sc_plug_ len	sc_pl_ver	sc_mil	sc_ind_lk	sc_total
25/1-1	3	0	0	0	0	0	2	–6	0	0	0	2	1.00
25/1-2	3	0	0	0	0	0	2	–6	0	0	0	2	1.00
25/1-3	3	0	0	0	0	0	2	–6	0	0	0	2	1.00
25/1-5	3	0	0	0	0	0	2	–6	0	0	0	2	1.00
25/1-7	3	0	0	1	1	0	2	–5	1	0	0	2	5.00
25/1-8	3	0	0	1	1	0	2	–3	2	0	1	2	9.00
25/1-10	3	0	0	0	1	0	1	–4	3	0	0	2	6.00
30/10-1	2	0	0	0	0	0	1	–3	2	0	0	2	4.00
30/10-4	2	0	0	0	0	0	1	–2	0	0	0	2	3.00
30/10-5	3	0	0	0	1	2.4	1.5	3	3	3	1	2	19.90
Max value	**3**	**2**	**1**	**1**	**3**	**3**	**3**	**6**	**3**	**3**	**1**	**2**	**31.00**

data usually contain all details of the drilling and abandonment procedure summarized in a well completion report. P&A is then compared to the present regulations for NCS (NORSOK D-10, 2004). Twelve criteria are differently weighted, resulting in a final maximum score of 31. Higher scores indicate complete documentation of the drilling and abandonment procedure and a good P&A job following current regulations. Lower scores indicate missing documentation and/or poor P&A completion with respect to current regulations. Wells from Frigg Field get screening scores between 1 and 19.9 (Table 2). Low-scored wells require more attention and monitoring in the case of storage in this area.

Noninvasive monitoring of casing corrosion

Modeling approach and numerical model. For noninvasive monitoring, as we consider effects of the corrosion on the casing, we focus on CSEM, which is most sensitive to changes in electrical conductivity in the subsurface. Marine CSEM can be used for hydrocarbon exploration (Constable, 2010). It has been demonstrated to be potentially useful for well-integrity characterization by a small-scale experiment (Wilt et al., 2020) and synthetic modeling (Romdhane et al., 2022b). Wilt et al. (2020) demonstrate that time-domain reflectometry for onshore wells is relevant when the steel casing is used as an antenna. Romdhane et al. (2022b) show that CSEM enables the identification of 10 m long sections of corroded casing at 150 m depth by using a conventional CSEM acquisition layout in a marine environment. To improve probing depth and characterize corroded sections at greater depth, we are testing the use of the casing as an antenna by plugging a dipole antenna into the casing. This method, aimed at energizing the steel casing at the wellhead and focusing on time-lapse changes due to well damage, is known as the top-casing method (Wilt et al., 2018; Um et al., 2019; Wilt and Nieuwenhuis, 2019; Wilt et al., 2020).

Modeling CSEM signal is carried out with COMSOL Multiphysics software. In a first approximation, we only consider conductive effects in the model, therefore neglecting inductive effects. This amounts to solving, in the frequency domain, the set of equations:

$$\boldsymbol{J} = (\sigma + i\omega\varepsilon_0\varepsilon_r)\boldsymbol{E}, \quad (1)$$

$$\nabla \cdot \boldsymbol{J} = Q, \text{ and} \quad (2)$$

$$\boldsymbol{E} = -\nabla V, \quad (3)$$

where $\boldsymbol{E}$ is the electric field, V is the electric potential, Q is the charge density, and $\boldsymbol{J}$ is the total electric current density. Here, σ, ε_r, and ε_0 are the medium properties governing wave propagation: electrical conductivity, relative dielectric permittivity, and vacuum electrical permittivity, respectively. In addition, ω is the angular frequency.

The modeling domain is surrounded by absorbing boundary conditions to avoid unwanted reflections due to the use of a limited bounded simulation domain. By taking advantage of the symmetry of the geometry along the plane of the well and the dipole, computational requirements can be reduced by half. The model is meshed with a tetrahedral mesh (Figure 3).

We use a well model from the P&A report (Figure 1c) to build a numerical model for CSEM modeling. The cylindrical well elements, radially layered to accommodate different wellbore and casing sizes, are enclosed in a large cylindrical domain with a radius of 1500 m. The radial spacing between metal casings is fully resolved in the geometry. The metal casings themselves are modeled as thin layers, with an effective formulation that accounts for their thickness without requiring a mesh (known as the electric shielding boundary condition in COMSOL Multiphysics software).

Corrosion can be introduced to any metal casing by reducing the local conductivity in any arbitrary cylindrical segment of the casing (Wilt et al., 2020). For this work, we focus on the innermost casing and look at a 100 m long corroded section (Figure 3). The uncorroded steel conductivity is set to $\sigma = 4 \times 10^6$ S/m. Corroded casing conductivity can take values as low as $\sigma = 4 \times 10^3$ S/m (Wilt et al., 2020). Therefore, the thin layer approximation is warranted considering two factors. First, the conductivity of the casings is much larger than the conductivity of the surrounding materials (which are on the order of 1 S/m). Second, given a casing thickness of 12 mm, the skin depth at the operating frequency of 10 Hz (for casings' relative permittivities and permeabilities of 1 and 10) varies from 20 mm in the uncorroded case to 800 mm in the case with the highest corrosion.

The whole geometry is also layered, following the geometrical changes in the well elements, with the inclusion of a water layer and an air layer at the top. Properties of the rock formation are also assumed to be layered based on a 1D model of conductivity from the resistivity log. Relative permittivity values are taken to be 6 for the formation, 2.2 for cement, 78.4 for water, and 1 for steel. EM fields are excited via a 1 km long dipole on the seabed (with one end connected to the 13⅜-inch steel casing, which reaches the seafloor and goes as deep as 1000 m below the sea surface) and a return electrode on the seafloor. The dipole is driven by imposing a potential difference of 1 kV across its length at an operating frequency of 10 Hz. We generate a set of models with different corrosion sections and different levels of corrosion, and we compare the electric field components. Figure 3 summarizes the setup with details of the well elements, rock formation conductivity, and mesh.

In the following subsection, we investigate the potential of this modeling approach in providing insight into the physics of signal propagation in the well structure, its interaction with the corroded region, and its propagation back to the seabed. This establishes a basis for further investigation of CSEM for corrosion monitoring and detection. In particular, given the approximations and simplifications introduced (especially in the omission of inductive effects) and the limited exploration of different excitation frequencies and configurations, absolute signal levels returned by the model are not yet interpreted against the capabilities of realistic instrumentation used in the field. For this reason, field magnitudes are reported in arbitrary units, and their usefulness is limited to relative comparison between different cases. The extension of the modeling to realistic signal levels and detection strategies is reserved for future work.

CSEM modeling results. With a linear voltage drop along the dipole on the seafloor as excitation, we investigate the changes in the electric field caused by different levels of corrosion in the innermost casing of the well by using the case with no corrosion as a baseline. We consider the scattered electric field, which is defined as the difference between the electric field for the case with no corrosion (i.e., intact casing, no changes in conductivity) and the case with corrosion, as our variable of interest. Results for a dipole connected to the third casing of the well and a 100 m long corroded section starting at a depth of 500 m are displayed in Figure 4. The figure shows how the entire well structure acts as an antenna,

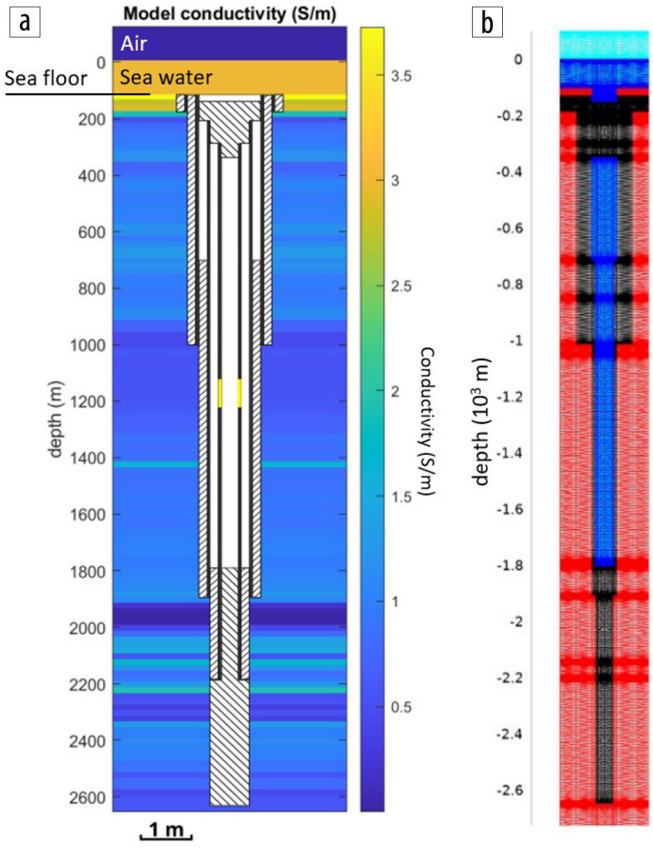

Figure 3. (a) Model of well elements and rock formation conductivity. In the well geometry, shaded areas indicate cement casing and plugs, thick black lines correspond to metal casings, and the yellow areas indicate an example location of a 100 m long corroded metal casing. White areas are filled with water. The lateral scale is not to scale versus the vertical scale. The conductivity model spans 1500 m horizontally, and the well is assumed to be located in the center. (b) Meshing in proximity of the well structure. Formation elements are in red, wellbore and sea water is in blue, cement is in black, and air is in cyan. Areas with denser mesh correspond to locations with small geometric features. Because of the different scales in the lateral and vertical directions, mesh elements appear distorted in the image.

with the corroded section at the center of current lines. The field excitation and the signature of the corroded casing are clearly visible. The reservoir layer at 1927 m depth (top Frigg Formation) has high resistivity compared to the conductive cap rock (Hordaland Group). We observe that a fair part of the EM energy is leaking in the reservoir, reducing the probing depth under this resistive layer. Similar behavior is observed by Heagy and Oldenburg (2019) when modeling a DC resistivity experiment. They find that larger resistivity contrasts between casing and rock formation will lead to a larger secondary response. Wilt et al. (2020) also emphasize that the background resistivity distributions can influence the recorded electric field at the surface and reduce the leak-off of current from the well casing into the rock formation.

To evaluate the possibility of detecting corrosion and its severity, we examine scattered fields at the seafloor along the radial direction from the well in the opposite direction of the dipole (corresponding to the positive x-axis in Figure 4). This is where signals can be measured by adapting conventional CSEM acquisition layouts. It is interesting to first look at how signal levels (i.e., scattered field magnitude) behave with varying distances

from the well and varying levels of corrosion. As one would expect, signal strength decays exponentially with distance (Figure 5). Heagy and Oldenburg (2019), Wilt et al. (2020), and Beskardes et al. (2021) observe similar phenomena: a decrease over distance when modeling the DC electrical part of the response. At the same time, the most significant changes in signal strength occur when casing conductivity is reduced to a factor of 10, with only a marginal signal increase for further reduction (right-hand side of Figure 6). This indicates that for a well structure with telescopic casings, even a moderate reduction in conductivity in the innermost casing displaces the currents toward other casings, significantly altering the field topology. Once this is achieved, additional decreases in the conductivity do not further alter the current distribution and only marginally affect the overall signal strength. This behavior is clearly visible in Figure 7, where a drop in conductivity in the corroded region leads to a significant current reduction in the innermost casing (the current is down 90%, with conductivity reduced by a factor of 10), while the currents increase in the second and third casings. The current increase is more localized in the second casing because of the immediate proximity to the corroded area with respect to the third casing. At larger corrosion levels, there is also a clear interplay between the second and third casings, with the current profile on the second casing displaying a local minimum at a depth of 550 m.

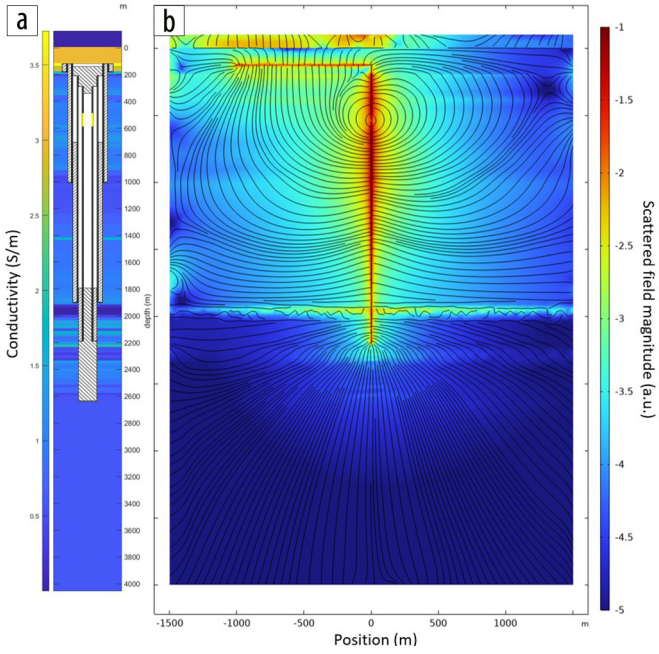

Figure 4. (a) Well structure and formation conductivity (more details in Figure 3). The corroded section is highlighted in yellow. (b) Scattered field magnitude in log scale and current lines (black lines) on the vertical plane along the well and the dipole for a 100 m long corroded section at a depth of 500 m with a conductivity of 4000 S/m. The scattered field components are defined as the difference between the field components in the case with corrosion and without corrosion. The dipole is visible as the horizontal line left of the well at a depth of 127 m. Field excitations are clearly propagating along the whole well structure, with current lines (in black) closing around the corroded section. Note how the reservoir (with high resistivity) shields the deeper portion of the model, where scattered fields are introduced via the casings below 2000 m.

Next, we consider how the signal at the seafloor is affected by the depth of the corroded region. For varying levels of corrosion, the location of the corroded region is varied from 350 to 1700 m, covering most of the innermost casing. Modeling larger depths is technically possible, but the signal levels at the seafloor are very low and produce noisy data. For a meaningful comparison between different locations of the corroded region and to evaluate relative changes in the local fields, we look at the signal gain g_i rather than the scattered field. This is defined for each field component i as $g_i = 20\log_{10}\left(1 - \frac{E_{scattered}}{E_{intact}}\right)$, where $E_{\text{scattered}}$ and E_{intact} are the scattered electric field and the electric field of the intact casing case, respectively. Results are reported in Figure 8 for measurements performed on the seafloor 300 m away from the well. A local minimum is present at a depth of 800 m, corresponding to the location of two overlapping cement casings in the well structure. The signal gain increases as part of the corroded section exits this area, resuming its decline below 1000 m depth when only one cement casing is present.

The results for a complete set of corrosion levels and depths of the corroded region are reported in Figure 9. They confirm the qualitative behavior described in Figures 7 and 8, with gain rapidly increasing with a conductivity of the corroded region at approximately 10^6 S/m and a local minimum at depths between 700 and 900 m where the two cement casings overlap.

Discussion

These results suggest that the top-casing CSEM survey of a complex well geometry that is typical for deep exploration wells is sensitive to the effects of corrosion to the steel casings when modeled as a reduction in electrical conductivity. Already, with a reduction of a factor of 10, the current distribution is significantly modified, with current paths shifting from the more resistive corroded region to the more conductive casings in its proximity. While further corrosion in the same location does not alter the current paths, it does generate a marginally stronger signal at the seafloor. In addition, it has been shown that the EM signal of the corroded well carries information about the location

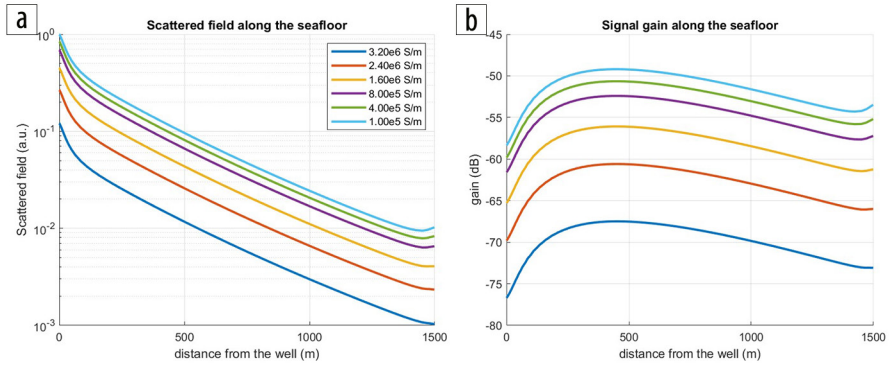

Figure 5. (a) Scattered field magnitude and (b) signal gain along the seafloor compared with the distance from the wellhead for different values of corroded section conductivity. The decay of field magnitude with distance is mostly exponential, as expected, while signal gain peaks between 300 and 500 m from the well.

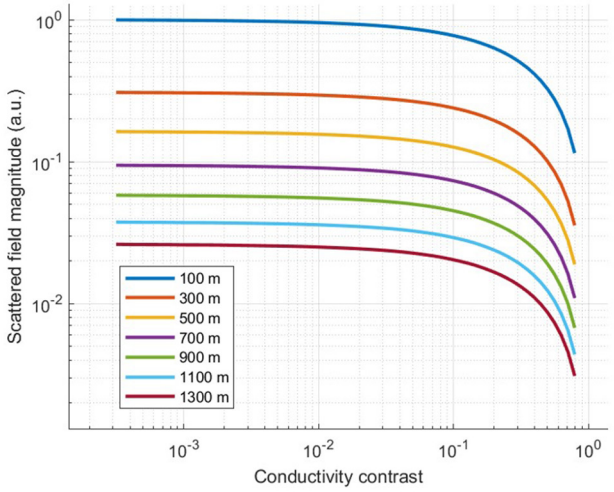

Figure 6. Scattered field magnitude compared with varying conductivity of the corroded region at different distances from the well on the seafloor. Note how the largest changes in signal occur on the right-hand side of the plot, where conductivity is reduced by a factor of 10. Varying the distance to the well amounts to a simple scaling factor, suggesting no significant qualitative difference between locations.

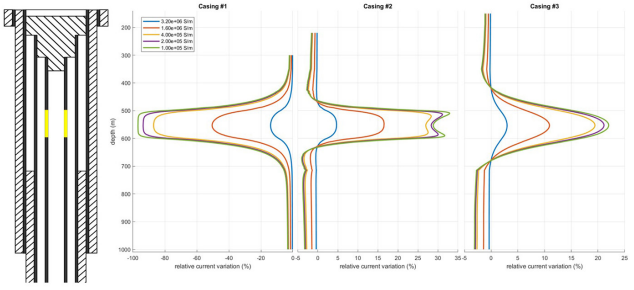

Figure 7. Relative variation in the surface current along the different casings with varying degrees of corrosion in a 100 m long section highlighted in the well schematic on the left (to scale with the vertical axes of the plots). As conductivity in the corroded region drops, so does the current in the first casing. This corresponds to an increase in the surface currents in the second and third casings.

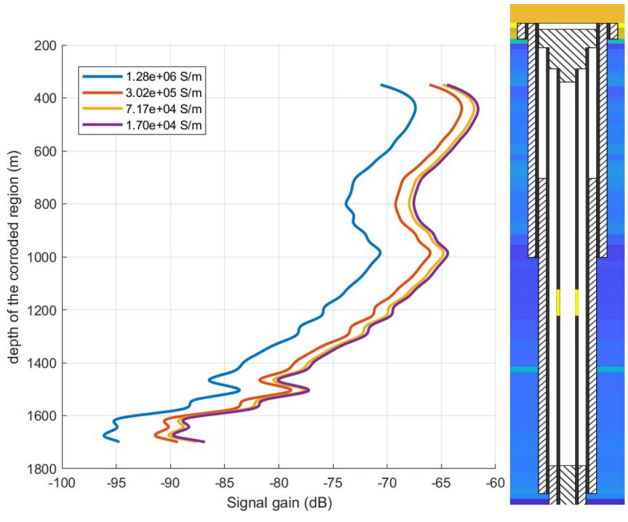

Figure 8. Signal gain versus depth of the top of the corroded region for different corrosion levels measured on the seafloor 300 m away from the well. The gain drops to a local minimum as the corroded region approaches the area between 700 and 1000 m depth where two cement casings overlap, reducing the ability of the currents to bypass the corroded region via other casings.

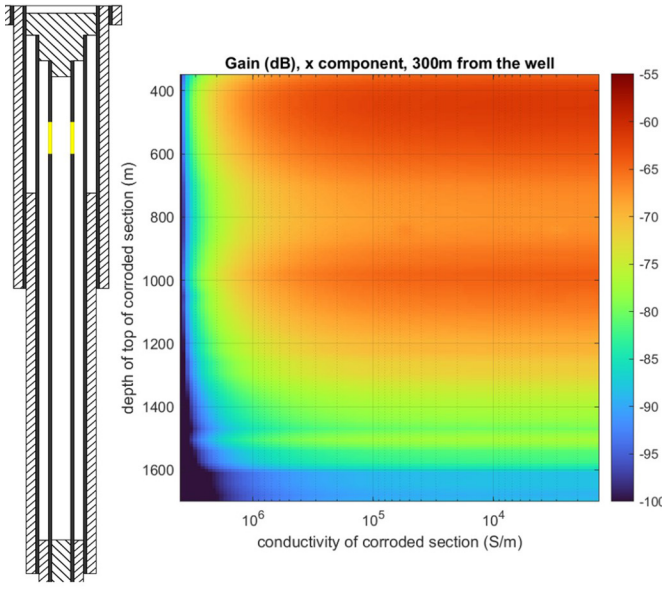

Figure 9. Gain for the *x* component of the electric field as measured on the seafloor 300 m away from the well when the dipole is connected to the fourth casing for different values of the conductivity and depth (of the top boundary) of the corroded section. The well structure, to scale in the vertical direction, is provided as reference.

of the corroded region itself, namely with a drop in seafloor signal when the corroded section is located behind two overlapping cement casings. This suggests that with knowledge of the well structure and its uncorroded signal (baseline model), it can be possible to determine not only whether corrosion has occurred and its severity, but also estimate its location. Similar conclusions are drawn by Wilt et al. (2020) for onshore wells. However, in order to evaluate the expected signal levels and compare them with existing detection capabilities, a more comprehensive modeling approach will be required (i.e., with the inclusion of inductive effects and the investigation of a range of excitation frequencies). A more detailed study of the signature of corrosion on different casings, rather than on the innermost casing alone, would be of interest. It would also be interesting to study the signature of multiple areas of corrosion in the same well geometry and the length of the corroded section (Beskardes et al., 2021). Finally, implementing realistic sources will allow us to quantify the observed changes at the seabed and compare them with EM noise floors (Pidlisecky et al., 2007; Grayver et al., 2013) relative to CSEM data uncertainty (Mittet and Morten, 2012). This would enable us to study and optimize detectability of changes by adapting acquisition layouts (including potentially downhole layouts) and testing other frequencies and field components.

In general, the suggested modeling approach and its immediate extension provide a promising strategy for the future detection and monitoring of corrosion in P&A wells. The capability of accessing and understanding the details of signal propagation and complex interactions within the well structure, and the ease of implementing any well geometry and local formation properties, can be valuable in optimizing the approach to specific challenges. Earlier studies (Romdhane et al., 2022a) also show that CSEM can be used to characterize shallow cement plugs (environment plugs close to the surface). For assessment of overburden and

reservoir plugs, tube wave generations at the wellhead and recording of time-lapse changes along the well or at the wellhead are valuable methods to be tested.

Conclusions

The North Sea is considered to be a potential major hub for CO_2 and energy storage. Shut-down fields such as Frigg Field are relevant storage locations due to their well-characterized reservoir and cap-rock formations and large storage capacities. However, CO_2-injection-related reservoir models from Frigg Field indicate that exploration legacy wells are situated at critical locations within the field. Independent from injection locations, these wells will be reached by a migrating CO_2 plume. Using Frigg Field (as an example of a shut-down field) for large-scale storage requires assessing and monitoring legacy wells. Characterization of the well elements, especially cement plugs and casings, is required to ensure that old legacy wells are not a containment threat and can act as a leakage path. Top-casing CSEM modeling shows promising results in characterizing and monitoring the casing corrosion. The probing depth depends on the casing structure and the rock formation conductivity but seems to be good enough to be a realistic method to use at field scale. More in-depth modeling and field-scale tests are required to quantify the magnitude of the changes due to casing corrosion. If such a CSEM survey is carried out at regular times, screening for time-lapse changes in the signal will allow us to identify any change in the casing corrosion, monitor possible corrosion by corrosive fluids (CO_2), and detect possible leakages early (migration of CO_2 up along the legacy well corroding higher sections of the well casing). TLE

Acknowledgments

This work was performed with support from the Research Council of Norway (TOPHOLE project Petromaks2-KPN 295132, EM4CO2 Climit-KPN 295212/E20, FP HYSTORM 315804, and NCCS Centre 257579/E20).

Data and materials availability

Data associated with this research are confidential and cannot be released.

Corresponding author: bastien.dupuy@sintef.no

References

Akerboom, S., S. Waldmann, A. Mukherjee, C. Agaton, M. Sanders, and G. J. Kramer, 2021, Different this time? The prospects of CCS in the Netherlands in the 2020s: Frontiers in Energy Research, **9**, https://doi.org/10.3389/fenrg.2021.644796.

Bertolini, L., B. Elsener, P. Pedeferri, E. Redaelli, and R. Polder, 2003, Corrosion of steel in concrete: Prevention, diagnosis, repair: Wiley.

Beskardes, G. D., C. J. Weiss, E. Um, M. Wilt, and K. MacLennan, 2021, The effects of well damage and completion designs on geoelectrical responses in mature wellbore environments: Geophysics, **86**, no. 6, E355–E366, https://doi.org/10.1190/geo2020-0702.1.

Cahill, A. G., and P. S. G. Samano, 2022, Prioritizing stewardship of decommissioned onshore oil and gas wells in the United Kingdom based on risk factors associated with potential long-term integrity: International Journal of Greenhouse Gas Control, **114**, https://doi.org/10.1016/j.ijggc.2021.103560.

Choi, Y.-S., D. Young, S. Nešić, and L. G. Gray, 2013, Wellbore integrity and corrosion of carbon steel in CO_2 geologic storage environments: A literature review: International Journal of Greenhouse Gas Control, **16**, S70–S77, https://doi.org/10.1016/j.ijggc.2012.12.028.

Constable, S., 2010, Ten years of marine CSEM for hydrocarbon exploration: Geophysics, **75**, no. 5, 75A67–75A81, https://doi.org/10.1190/1.3483451.

De Leebeeck, A., 1987, The Frigg Field reservoir: Characteristics and performance, *in* J. Kleppe, ed., North Sea oil and gas reservoirs: Springer Netherlands, 89–100.

Eliasson, P., E. Barros, P. E. S. Bergmo, J. Blackford, S. Carpentier, P. Cerasi, B. Dupuy, et al., 2021, Pressure control and conformance management for safe and efficient CO_2 storage — Lessons learned in the Pre-ACT project: Presented at the 15th Greenhouse Gas Control Technologies Conference.

Emmel, B., and B. Dupuy, 2021, Dataset of plugging and abandonment status from exploration wells drilled within the Troll gas and oil field in the Norwegian North Sea: Data in Brief, **37**, https://doi.org/10.1016/j.dib.2021.107165.

Emmel, B., B. Bjørkvik, T. L. Frøyen, P. Cerasi, and A. Stroisz, 2023a, Evaluating the hydrogen storage potential of shut down oil and gas fields along the Norwegian Continental Shelf: International Journal of Hydrogen Energy, **48**, 24,385–24,400, https://doi.org/10.1016/j.ijhydene.2023.03.138.

Emmel, B., A. Romdhane, B. Dupuy, S. Zonetti, and A. Barrabino, 2023b, De-risking legacy well integrity to unlock storage potential of the Frigg Field, North Sea Norway: 84th Annual Conference and Exhibition, EAGE, Extended Abstracts, https://doi.org/10.3997/2214-4609.202310753.

Gasda, S. E., S. Bachu, and M. A. Celia, 2004, Spatial characterization of the location of potentially leaky wells penetrating a deep saline aquifer in a mature sedimentary basin: Environmental Geology, **46**, 707–720, https://doi.org/10.1007/s00254-004-1073-5.

Grayver, A.V., R. Streich, and O. Ritter, 2013, Three-dimensional parallel distributed inversion of CSEM data using a direct forward solver: Geophysical Journal International, **193**, no. 3, 1432–1446, https://doi.org/10.1093/gji/ggt055.

Hamza, A., I. A. Hussein, M. J. Al-Marri, M. Mahmoud, R. Shawabkeh, and S. Aparicio, 2021, CO_2 enhanced gas recovery and sequestration in depleted gas reservoirs: A review: Journal of Petroleum Science and Engineering, **196**, https://doi.org/10.1016/j.petrol.2020.107685.

Hannis, S., J. Lu, A. Chadwick, S. Hovorka, K. Kirk, K. Romanak, and J. Pearce, 2017, CO_2 storage in depleted or depleting oil and gas fields: What can we learn from existing projects?: Energy Procedia, **6**, 5680–5690, https://doi.org/10.1016/j.egypro.2017.03.1707.

Heagy, L. J., and D. W. Oldenburg, 2019, Direct current resistivity with steel-cased wells: Geophysical Journal International, **6**, no. 1, https://doi.org/10.1093/gji/ggz281.

Holloway, S., C. Rochelle, K. Bateman, J. Pearce, H. Baily, and R. Metcalfe, 1996, The underground disposal of carbon dioxide: Final report: British Geological Survey.

IPCC, 2005, Carbon dioxide capture and storage: Cambridge University Press.

ISO, 2022, ISO 27914:2017, https://www.iso.org/standard/64148.html, accessed 3 May 2023.

Koning, M., V. Zikovic, K. Van der Valk, R. Pawar, J. Williams, N. Opedal, and A. Dudu, 2023, Development of a screening framework for re-use of existing wells for CCUS projects considering regulatory, experimental and technical aspects: Presented at the Middle East Oil, Gas and Geosciences Show.

Lothe, A. E., P. E. Bergmo, and A.-A. Grimstad, 2019, Storage resources for future European CCS deployment: A roadmap for a Horda CO_2 storage hub, offshore Norway: Presented at the 10th Trondheim Conference on CO_2 Capture, Transport and Storage.

Mittet, R., and J. P. Morten, 2012, Detection and imaging sensitivity of the marine CSEM method: Geophysics, **6**, no. 6, E411–E425, https://doi.org/10.1190/geo2012-0016.1.
NMPE, 2020, Longship — Carbon capture and storage: Norwegian Ministry of Petroleum and Energy.
NORSOK D-10, 2004, d-010r3.pdf, https://www.standard.no/pagefiles/1315/d-010r3.pdf, accessed 2 November 2022.
Norwegian Petroleum Directorate, 1991, Well 25/1-8-SR final report, https://factpages.npd.no/pbl/wellbore_documents/1644_25_1_8_SR4_completion_report,pdf, accessed 26 October 2023.
Norwegian Petroleum Directorate, 2014a, CO_2 atlas for the Norwegian Continental Shelf, http://www.npd.no/en/Publications/Reports/Compiled-CO_2-atlas/, accessed 25 October 2023.
Norwegian Petroleum Directorate, 2014b, Regulations relating to exploitation of subsea reservoirs on the continental shelf for storage of CO_2 and relating to transportation of CO_2 on the continental shelf, https://www.npd.no/en/regulations/regulations/exploitation-of-subsea-reservoirs-on-the-continental-shelf-for-storage-of-and-transportation-of-co/, accessed 26 October 2023.
Norwegian Petroleum Directorate, 2023, Frigg Field factpages, https://factpages.npd.no/en/field/PageView/ShutDown/43555, accessed 22 September 2023.
Osmond, J. L., M. J. Mulrooney, N. Holden, E. Skurtveit, J. I. Faleide, and A. Braathen, 2022, Structural traps and seals for expanding CO_2 storage in the northern Horda platform, North Sea: AAPG Bulletin, **106**, no. 9, 1711–1752, https://doi.org/10.1306/03222221110.
Pawar, R., L. Brunner, K. van der Valk, L. van Bijsterveldt, D. Harp, B. Chen, L. Cangemi, et al., 2021, A screening tool for assessing feasibility of re-using existing oil and gas wells for CCUS operations: Presented at the 15th Greenhouse Gas Control Technologies Conference.
Pidlisecky, A., E. Haber, and R. Knight, 2007, RESINVM3D: A 3D resistivity inversion package: Geophysics, **72**, no. 2, H1–H10, https://doi.org/10.1190/1.2402499.
Ringrose, P. S., and T. A. Meckel, 2019, Maturing global CO_2 storage resources on offshore continental margins to achieve 2DS emissions reductions: Scientific Reports, **9**, https://doi.org/10.1038/s41598-019-54363-z.
Romdhane, A., B. Emmel, S. Zonetti, B. Dupuy, K. Gawel, L. Edvardsen, and M. H. Bhuiyan, 2022a, Screening, monitoring, and remediation of legacy wells to improve reservoir integrity for large-scale CO_2 storage — An example from the Smeaheia structure in the northern North Sea: Frontiers in Energy Research, **10**, https://doi.org/10.3389/fenrg.2022.826100.
Romdhane, A., B. Emmel, S. Zonetti, and B. Dupuy, 2022b, Screening and non-invasive geophysical monitoring of legacy wells integrity for offshore CO_2 storage: Presented at the 16th Greenhouse Gas Control Technologies Conference.
Statistics Norway, 2023a, Emissions to air, https://www.ssb.no/en/natur-og-miljo/forurensning-og-klima/statistikk/utslipp-til-luft, accessed 26 October 2023.
Statistics Norway, 2023b, Production and consumption of energy, energy balance and energy account, https://www.ssb.no/en/energi-og-industri/energi/statistikk/produksjon-og-forbruk-av-energi-energibalanse-og-energiregnskap, accessed 26 October 2023.
Sun, Q., W. Ampomah, E. J. Kutsienyo, M. Appold, B. Adu-Gyamfi, Z. Dai, and M. R. Soltanian, 2020, Assessment of CO_2 trapping mechanisms in partially depleted oil-bearing sands: Fuel, **278**, https://doi.org/10.1016/j.fuel.2020.118356.
Thommessen, C., M. Otto, F. Nigbur, J. Roes, and A. Heinzel, 2021, Techno-economic system analysis of an offshore energy hub with an outlook on electrofuel applications: Smart Energy, **3**, https://doi.org/10.1016/j.segy.2021.100027.
Total, 2011, Frigg Field cessation plan: Close out report, https://assets.publishing.service.gov.uk/government/uploads/system/uploads/attachment_data/file/1069924/frigg-close-out-report.pdf, accessed 26 October 2023.
Um, E. S., J. Kim, M. J. Wilt, M. Commer, and S.-S. Kim, 2019, Finite-element analysis of top-casing electric source method for imaging hydraulically active fracture zones: Geophysics, **84**, no. 1, E23–E35, https://doi.org/10.1190/geo2018-0451.1.
Urosevic, M., R. Pevzner, A. Kepic, P. Wisman, V. Shulakova, and S. Sharma, 2010, Time-lapse seismic monitoring of CO_2 injection into a depleted gas reservoir — Naylor Field, Australia: The Leading Edge, **29**, no. 2, 164–169, https://doi.org/10.1190/1.3304819.
Vrålstad, T., A. Saasen, E. Fjær, T. Øia, J. D. Ytrehus, and M. Khalifeh, 2019, Plug & abandonment of offshore wells: Ensuring long-term well integrity and cost-efficiency: Journal of Petroleum Science and Engineering, **173**, 478–491, https://doi.org/10.1016/j.petrol.2018.10.049.
Wilt, M., and G. Nieuwenhuis, 2019, Wellbore integrity mapping using well-casing electrodes and surface-based electromagnetic fields: U.S. Patent Application 16/337,010.
Wilt, M., G. Nieuwenhuis, K. Maclennan, and E. Um, 2018, Casing-integrity mapping using top-casing electrodes and surface based EM fields: 88th Annual International Meeting, SEG, Expanded Abstracts, 858–862, https://doi.org/10.1190/segam2018-2983425.1.
Wilt, M. J., E. S. Um, E. Nichols, C. J. Weiss, G. Nieuwenhuis, and K. MacLennan, 2020, Casing integrity mapping using top-casing electrodes and surface-based electromagnetic fields: Geophysics, **85**, no. 1, E1–E13, https://doi.org/10.1190/geo2018-0692.1.